A laser-aided prealigned pinhole collimator for synchrotron x rays

Benjamin Chu,[a] Paul J. Harney, Yingjie Li, Kung Linliu, and Fengji Yeh
Department of Chemistry, State University of New York at Stony Brook, Stony Brook, New York 11794-3400

Benjamin S. Hsiao
Experimental Station, Fibers Department, E.I. DuPont de Nemours and Co., P.O. Box 80302, Wilmington, Delaware 19880-0302

(Received 16 September 1993; accepted for publication 3 December 1993)

A pinhole small-angle x-ray scattering (SAXS) instrument was constructed at the SUNY X3A2 beamline, National Synchrotron Light Source, Brookhaven National Laboratory. The three pinholes were mounted in a thick-walled stainless steel pipe and *prealigned* by using a portable laser source and a charge-coupled device (CCD) area detector. After the prealignment, incorporation of the collimator to the synchrotron x-ray source required only maximization of the incident x-ray intensity passing through the pinholes, which could be done easily by using a scintillation counter after proper attenuation. The entire synchrotron SAXS instrument setup took only a few hours even without stepping motor control for the pinhole collimator unit. By combining this collimator with a CCD-based x-ray area detector which could be assembled by using commercially available components, the SAXS instrument showed good performance for structural scales up to an order of 100 nm. The CCD-based x-ray area detector used a computer- (or manually) controlled intensified unit with a variable gain setting in order to accommodate the changing x-ray flux and to protect the detector from over exposure, a necessary feature for operation of an area detector at a synchrotron light source.

I. INTRODUCTION

With the advent of high-flux synchrotron x-ray sources, small angle x-ray scattering (SAXS) has become a powerful technique in structural studies of a variety of materials.[1–3] As the synchrotron radiation source in combination with a focusing mirror has directional collimation, the pinhole collimator[4–21] offers more versatility because of its ability to investigate anisotropic systems. It also makes the desmearing effect less serious. However, the alignment of a pinhole collimator is more delicate in order to be able to reach the small scattering angles. Furthermore, synchrotron beamlines are usually shared by users with different instrumentation requirements. With tight beam-time schedules, it is desirable to minimize the time for instrumentation setup. Earlier, our group modified a Kratky block collimation system and adapted it successfully to the SUNY X3A2 beamline, National Synchrotron Light Source (NSLS), Brookhaven National Laboratory (BNL).[22] One of the unique features of a Kratky collimation system is that the collimator is *prealigned* as one integral unit. In this article, we report a successful implementation of the same concept, i.e., to construct a *prealigned* pinhole collimation system for the synchrotron source.

In order to maximize the efficiency of the synchrotron SAXS instrument with our laser-aided prealigned pinhole collimator, a charge-coupled device (CCD) based area detector, made of commercially available components, has also been developed. The CCD-based area detectors have several desirable qualities,[23–30] such as a relatively large collection area, high sensitivity, high quality of images, and fast readouts. The last property is particularly desirable for time-resolved experiments where the x-ray intensity may change rapidly. In this respect, we have also provided a computer-controlled gain for the image intensifier, so that large variations in the x-ray intensity during an experiment can be accommodated. Furthermore, the detector is protected when the intensity becomes too strong.

II. LASER-AIDED PREALIGNMENT OF A THREE-PINHOLE COLLIMATOR

Figure 1 shows a schematic diagram of a three-pinhole collimation geometry. The first and second pinholes define the incident beam. The third guard pinhole blocks the parasitic scattering due to the edge scattering from the second pinhole. It is noted that due to intrinsic convergence of the synchrotron beam, the incident flux is often controlled mainly by the size of the first pinhole. In order to achieve a high angular resolution, the guard pinhole must be designed and placed in such a way that it is close, but not touching the incident beam.[31]

The smallest angle one could reach without a serious parasitic scattering problem, θ_s, can be described by the relation

$$\theta_s=\frac{d_2+d_3}{2l_2}+\frac{d_3}{2l_3}+\frac{d_s}{2l_3}, \tag{1}$$

where d_s denotes a finite size for the detector element, and $d_3[\equiv(d_1+d_2)l_2/l_1+d_2]$ depends on l_1, l_2, d_1, and d_2. Based on the nature of the samples of interest and a compromise between the incident intensity and the angular resolution, we chose the following parameters: $l_1=l_2=609$

[a]Author to whom correspondence should be addressed.

 0034-6748/94/65(3)/597/6/$6.00

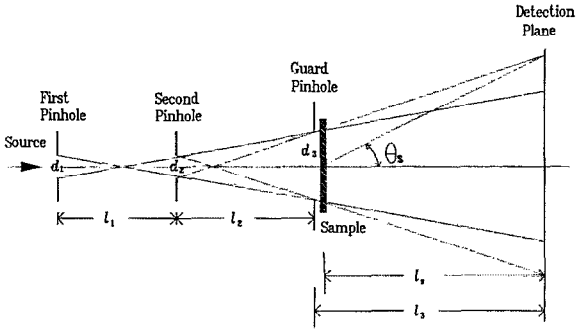

FIG. 1. Schematic diagram of a pinhole collimation geometry.

mm, $d_1=d_2=0.3$ mm. Therefore, d_3 should be slightly larger than 0.9 mm. We used $d_3=1.0$ mm and $l_s\approx l_3=1030$ mm. Theoretically, the pinhole collimation geometry should yield a θ_s of 1.62 mrad for our CCD-based area detector ($d_s=0.135$ mm) and a θ_s of 1.58 mrad for our Braun detector ($d_s=0.046$ mm).

A laser drilling technique was used to produce slightly tapered pinholes of different diameters with smooth edges on tantalum disks. The first and third pinhole disks were placed directly into the opposite ends of a ~1.2 m long stainless steel pipe (i.d.=6.35 mm and o.d.=19.05 mm). Threaded end caps with 3.2 mm diameter openings and rubber o-rings were used to secure the pinholes. A slot was cut into the center of the pipe to accommodate the second adjustable pinhole insert. Six set screws were used for fine tuning and securing the insert.

Figure 2 shows a schematic diagram for the prealignment of the pinhole collimator. In this setup, the CCD area detector (see Sec. III) was used to provide two-dimensional data for both the beam shape and its intensity pattern.

The prealignment procedure is described as follows. With the end caps in place, the empty tube was mounted on two x-y positioning stages and coarsely aligned. The guard pinhole was first inserted into the tube, and its position was set by maximizing the intensity and, at the same time, creating a circular, symmetric image which had a Gaussian beam pattern. The subsequent insertion of the first pinhole reduced the total intensity slightly. The first pinhole was positioned by again generating a symmetric

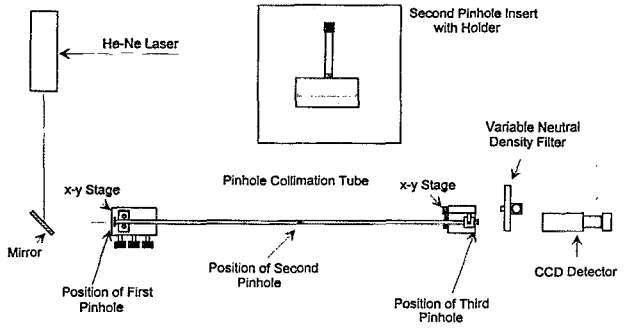

FIG. 2. Schematic diagram of prealignment of a block pinhole collimator by using a laser source (Spectra-Physics Model 133 He-Ne laser with $\lambda=632.8$ nm) and a CCD detector (Electrim Corp. EDC-1000).

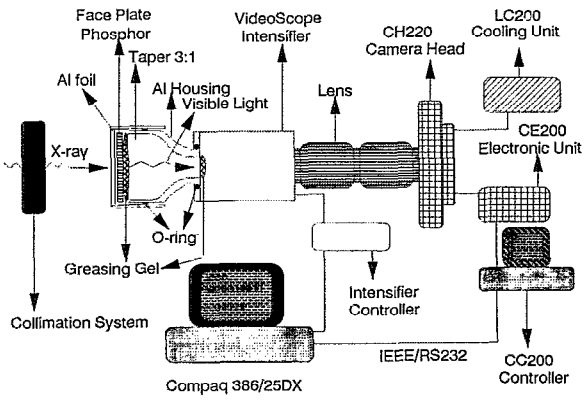

FIG. 3. Schematic diagram of CCD area detector.

beam pattern whose position was coincident with the peak position without the first pinhole in place. Finally, the second pinhole was inserted. Its position was adjusted by creating a symmetric Gaussian image with its peak position coincident with the one without the second pinhole in place. The tube was then sealed with Kapton windows for vacuum operation. This tube now becomes a self-contained, transportable, prealigned pinhole collimator unit, which weighs about 4 lb and is ready for the synchrotron setup.

III. CCD-BASED AREA DETECTOR

A. Description of detector

A schematic diagram of the detector is shown in Fig. 3. The area detector was composed of a phosphor-deposited face plate, a 3-in.-diam taper, an image intensifier unit with remote gain control, a double lens system, and a CCD camera. The key components and characteristics of the CCD detector are listed in Table I. The CCD detector could actually be used to detect x-rays and visible light. In the latter case, the aluminum foil and the phosphor-deposited face plate were removed from the system. The 3-in. fiber optic taper had a 3:1 ratio of front/back face.

The intensifier gain was first set at a nominal value of say 300 (relative gain value ranges from 0 to 1000). Once the CC200 controller received the x-ray intensity from the CH220 camera head, the PC computer could grab the maximum and the minimum intensity of the whole image immediately. If the maximum intensity was 16383 (saturated), there were three routes to protect the intensifier unit and the CCD chip:

(1) The PC could send a 5 V signal to the intensifier through an (analog-to-digital) A-D/D-A board (Dascon-1, Keithley Co.). The microchannel plate voltage would fall to 0 and disable the intensifier, as indicated by a light-emitting diode (LED) light. This procedure could protect both the CCD chip and the intensifier.

(2) If the VS-2525 were suddenly exposed to a bright input after a period of darkness, the rapid rise in current through the microchannel plate could also activate the brightness protection circuitry.

TABLE I. Key components of CCD area detector.

Component	Manufacture	Characteristics
(1) CCD camera	Photometrics Ltd.	Series 200: CC200 controller LC200 cooling unit CE200 electronic unit CH220 camera head 8 MB DRAM; 14 bits ADC Minimum exposure time 10^{-3} s
(2) CCD chip	Thompson CSF	TH7882CDA 23 μm×23 μm pixel size 576×384 pixels format
(3) Fiberoptic taper	Galileo Electro-Optics Co.	3-in. in diameter; 6-μm-diam fibers 3:1 magnification.
(4) Fiberoptic face plate	Galileo Electro-Optics Co.	6-μm diam fibers 1:1 no magnification
(5) Image intensifier	VideoScope International, Ltd.	VS2525; Gain could be controlled either manually or by computer
(6) Lens	Olympus	Lens combinations with (a) 100 mm/f2.8 and 50 mm/f1.2 (b) 100 mm/f2.8 and 35 mm/f2.8
(7) Phosphor	Thomas Electronics Co.	P45 Phosphor coating (BRE 1510) 6 μm particle size 10 mg/cm^2
(8) Optical coupling grease	Courtesy of Tom Lynch (VideoScope)	Refractive index ~1.7

(3) A reduced gain setting would be used so as to satisfy the condition: a preset value, say 16 000 < the brightest intensity per pixel in the scattering pattern.

Two sets of lenses could be selected: the 50 mm/f1.2 and 100 mm/f2.8 set yielded an effective area of 46×46 μm^2 per pixel at the back end of the taper, while the 35 mm/f2.8 and 100 mm/f2.8 set yielded an effective area of 66×66 μm^2 per pixel. The latter setting was used for covering the entire range of the 3-in. front-end optical fiber taper.

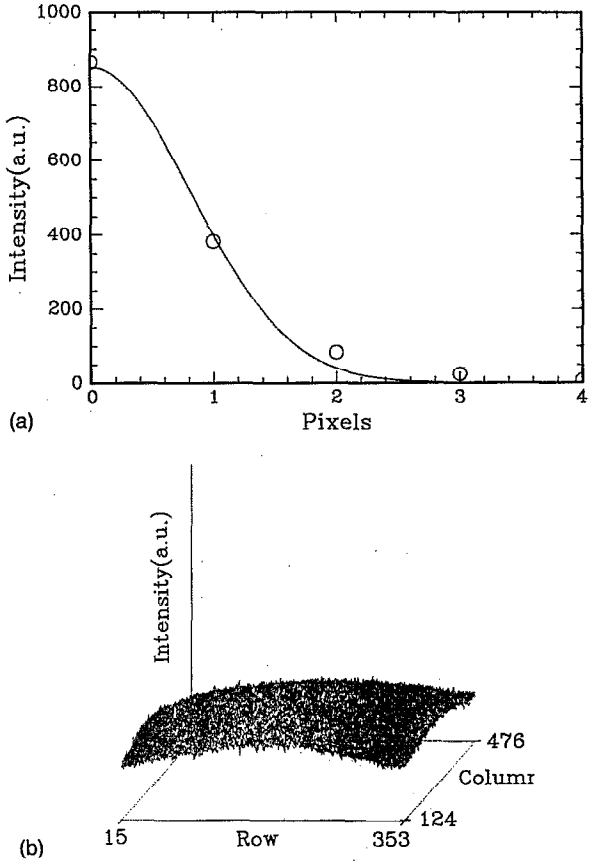

FIG. 4. (a) Point-spread function of CCD detector. Open circles represent the experimental data. Solid curve is the least squares fit of a Gaussian curve. The full width at half maximum (FWHM) is 1.6 pixel, corresponding to 220 μm at the phosphor. (b) 3D plot of flat field. The x-ray generator was operated at 10 kV/5 mA.

B. Detector performance check

1. Spatial resolution, uniformity of response, and linearity

The spatial resolution of the CCD detector was measured by placing a 25-μm-diam gold pinhole in front of the detector. Three images were taken, integrated radially and summed together. After averaging, the detector point-spread function was fitted to a Gaussian curve as shown in Fig. 4(a). The full width at half maximum (FWHM) was 1.6 pixels,[25,26,32] corresponding to an effective width of ~220 μm at the front end of the optical fiber taper. The pixel size of the CCD chip was 23 μm×23 μm, which represented an effective pixel size of 140 μm×140 μm at the phosphor by using a combined 50 mm/f1.2 lens and 100 mm/f2.8 lens, i.e., the lens set and the fiber taper provided about a 6× magnification at the phosphor. The resolution could be improved slightly by using the 50 mm/f1.2 and 35 mm/f2.8 set with further sacrifice on the effective angular range.

By locating the area detector toward the incident x-ray beam from a rotating anode x-ray source at a distance of 250 cm, an approximate flat field could be achieved and used to calibrate the spatial uniformity of response. A 3D

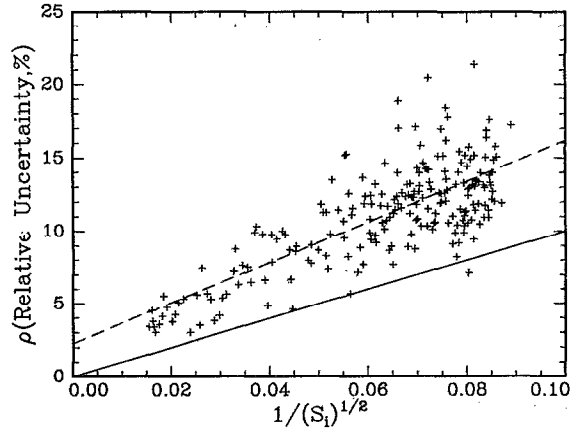

FIG. 5. Relative uncertainty ρ vs $(S_i)^{-1/2}$. Plus symbols represent an average of 20 experimental data points.

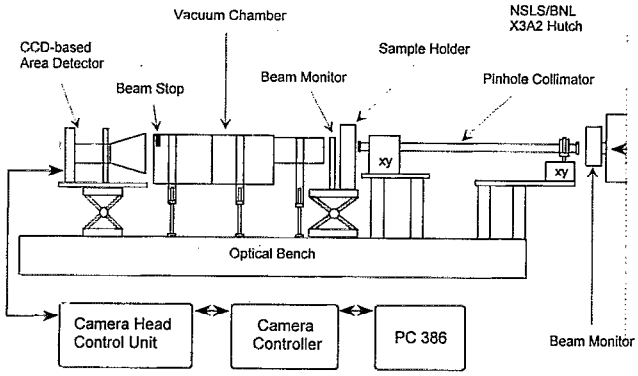

FIG. 6. Schematic diagram of the prealigned pinhole SAXS instrument at the SUNY X3A2 Beamline, National Synchrotron Light Source, Brookhaven National Laboratory.

picture of the flat field, as shown in Fig. 4(b), was used to correct the inhomogeneous response of different pixels.[10–13]

The relative spatial nonlinearity of the CCD detector was ±1 pixel over 100 pixels in both vertical and horizontal directions.

2. Detector quantum efficiency (DOE)

The detector quantum efficiency of a CCD detector is defined as follows:[33,34]

$$\mathrm{DQE}=(S_o/N_o)^2/(S_i/N_i)^2, \tag{2}$$

where S, N, and subscripts o, i represent the total integrated signal, RMS (rooted-mean-square) integrated noise, output and input of the signal, respectively. The incident x-ray photons were assumed to follow the Poisson distributions, $N_i=S_i^{1/2}$ and $S_o=G\,S_i$ with G being the gain. DQE was then related to the detector output uncertainty $\rho(=N_o/S_o)$ by the relation

$$\mathrm{DQE}=1/(\rho^2 S_i). \tag{3}$$

For an ideal detector (noiseless and loseless),[35] DQE is equal to 1, i.e., the output signal is equal to the input signal. To determine ρ experimentally, we measured 20 times the main beam with 100 s exposure at an intensifier gain setting of 600. By subtracting the dark counts (I_{dark}) from the measured intensity (I), we obtained S_o. The standard deviation of S_o is

$$\sigma_{so}=\left(\sum[(S_o)_j-\langle S_o\rangle]^2/(N-1)\right)^{1/2}, \tag{4}$$

with $\langle S_o\rangle=\Sigma(S_o)_j/N$, and $N=20$ for each pixel. A plot of detector output uncertainty ρ vs $(S_i)^{-1/2}$ is shown in Fig. 5. The dashed line designates a fitting of the experimental data, while the solid line represents the ideal case.

3. Pixel linearity of response and dynamic range

The pixel linearity of response of the CCD detector to the x-ray source power was measured by attenuating the incident x-ray beam with aluminum foil of different thickness at an x-ray power source setting of 20 kV/5 mA and an intensifier setting of 485 for the relative gain. The aluminum foil in front of the taper for blocking the visible light had a loss of about 22% at $\lambda=0.154$ nm. The average relative nonlinearity in the response of each pixel was less than 0.1% over a factor of 10 in each pixel. With the data for the pixel linearity of response and spatial uniformity of response, the distortion in the sensitivity and the uniformity of each pixel could be corrected.

The dynamic range of an imager is defined as the ratio of the maximum to the minimum detectable signal in a pixel.[36] The range is comparable to the CCD-based x-ray area detector which we have constructed recently,[32] the main difference being a better light-gathering relay lens and a commercially integrated image intensifier for the present area detector.

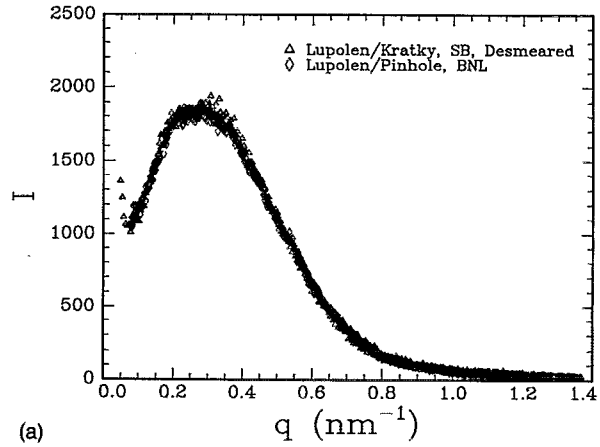

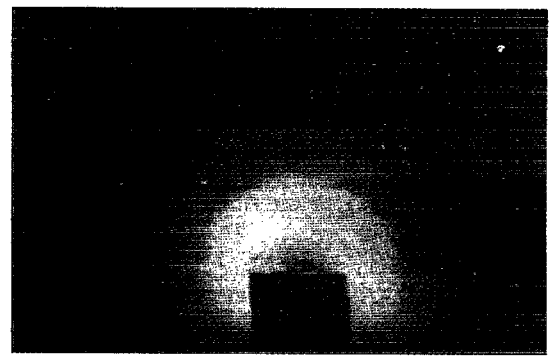

FIG. 7. Scattering patterns of a Lupolen standard by using (a) a Braun linear position-sensitive detector (measurement time 300 s). In (a) a SAXS profile of Lupolen from a commercial Kratky collimation system in combination with a gas proportional counter and a pulse height analyzer is also included. The measured SAXS profile from the Kratky collimator was desmeared by using the Lake algorithm. SB denotes the x-ray source as a rotating anode x-ray generator located at Stony Brook. BNL denotes the synchrotron x-ray source at X3A2, NSLS, BNL. (b) a CCD-based area detector (measurement time 60 s).

IV. SAXS INSTRUMENT DESCRIPTION AND TEST

Incorporation of the prealigned collimator to the synchrotron source could be performed by maximizing the x-ray intensity (using a scintillation counter) and by reconfirming the beam shape (using a CCD-based x-ray area detector). The total setup time took only a few hours on the first try even without remote x-y position controls.

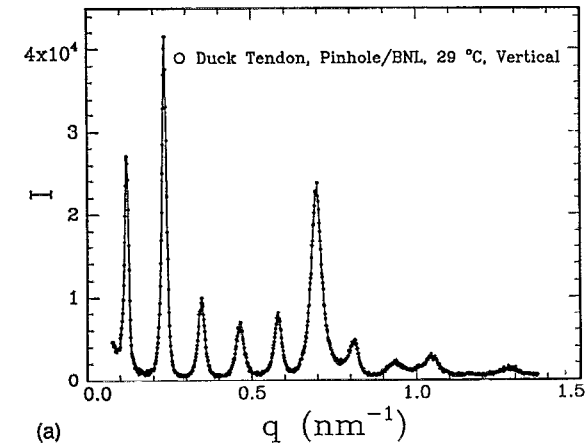

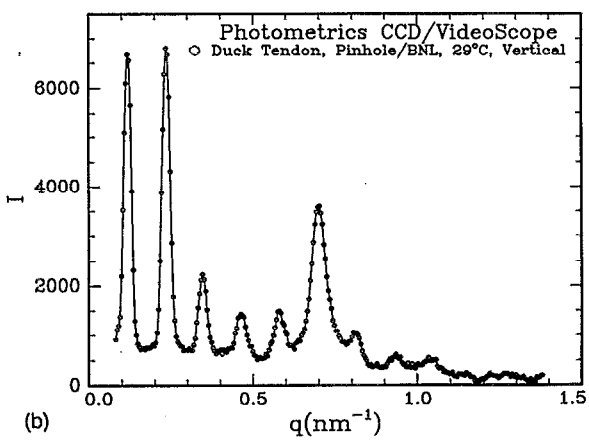

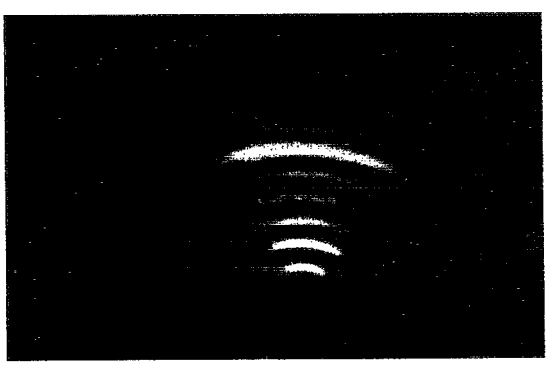

FIG. 8. Scattering patterns of a piece of duck tendon by using (a) a Braun linear position-sensitive detector (measurement time 300 s) and (b) a CCD-based area detector (measurement time 1000 s). Note that the lower resolution of the CCD-based area detector has distorted the base line and broadened the peak. (c) 2D image of the diffraction pattern of (b).

Figure 6 shows a schematic diagram of the pinhole SAXS instrument at the SUNY X3A2 beamline, NSLS, BNL. A Kratky rail could be used to accommodate a series of temperature-controlled sample holders for polymer crystallization, phase separation, and kinetic studies. In addition, a modified tensile stretching device was introduced into the setup for time-resolved SAXS and x-ray diffraction studies of films or fibers during stretching. A tantalum beam stop was mounted inside the vacuum chamber. The CCD-based area detector or a Braun linear position-sensitive detector could be used to collect the scattering data. A wavelength of 0.154 nm was used.

The pinhole system was tested by using both isotropic and anisotropic samples. Figures 7(a) and 7(b) show the scattering patterns of an isotropic Lupolen standard by using both the Braun and the CCD-based x-ray area detector. The one-dimensional profile for the pinhole system was compared with a profile of the same sample previously obtained by using a Kratky camera at the Stony Brook x-ray facility, as shown in Fig. 7(a). The smallest scattering angle we could reach was ~ 1.89 mrad. If we took the effects of the beam stop into account, the performance of the instrument met the theoretical design specification with $\theta_s = 1.62$ mrad for the pinholes tested.

Figures 8(a) and 8(b) show the scattering patterns of a duck tendon with Fig. 8(c) being the 2D image of the diffraction pattern of Fig. 8(b). The spacing calculated from the sixth peak was 54.2 nm, demonstrating the fine performance of the instrument. It should be noted that in the small-angle range, e.g., at $q < 0.1$ nm^{-1}, the Kratky collimator was more efficient for weakly scattering systems because of the design of its x-ray optics. For example, at $q = 0.1$ nm^{-1} (or $\theta \simeq 2.5$ mrad) the background parasitic scattering from the Kratky collimator was about 2.5 times lower than that of the pinhole collimator.

This instrument has been used for both static and time-resolved experiments.

ACKNOWLEDGMENTS

B.C. acknowledges the support of this project by the U.S. Department of Energy (Contract Nos. DEFG0286ER45237A009 and DEFG0589ER75515).

[1] T. P. Russell, in *Handbook on Synchrotron Radiation*, edited by G. Brown and D. E. Moncton (Elsevier, New York, 1991), Vol. 3.
[2] G. Elsner, Adv. Polym. Sci. **67**, 1 (1985).
[3] R. Gehrke, Top. Current Chem. **151**, 111 (1989).
[4] *Small Angle X-ray Scattering*, edited by O. Glatter and O. Kratky (Academic, New York, 1982).
[5] J. B. Leigh and G. Rosebaum, J. Appl. Cryst. **7**, 117 (1974).
[6] J. Hendrix, M. H. J. Koch, and J. Bordas, J. Appl. Cryst. **12**, 467 (1979).
[7] J. C. Hasegrove, A. R. Faruqi, H. E. Huxley, and U. W. Arndt, J. Phys. E **10**, 1035 (1977).
[8] G. B. Stephenson, Ph.D. thesis, Stanford University, 1982.
[9] G. B. Stephenson, Nucl. Instrum. Methods A **266**, 447 (1988).
[10] Y. Amemiya, K. Wakabayashi, T. Hamanaka, T. Wakabayashi, T. Matsushita, and H. Hashizume, Nucl. Instrum. Methods **208**, 471 (1983).
[11] D. Tchoubar, F. Rousseaux, C. Pons, and M. Lemonnier, Nucl. Instrum. Methods **152**, 301 (1978).
[12] J. M. Dubuisson, J. M. Dauvergne, C. Depautex, P. Vachette, and C. E. Williams, Nucl. Instrum. Methods A **246**, 636 (1986).
[13] S. Wakatsuki, K. O. Hodgson, D. Eliezer, M. Rice, S. Hubbard, N. Gillis, S. Doniach, and U. Spann, Rev. Sci. Instrum. **63**, 1736 (1992).
[14] H. G. Zachmann and C. Wutz, C. Polym. Prepr. **33**, 261 (1992).
[15] K. A. Cogan, A. P. Gast, and M. Capel, Macromolecules **24**, 6512 (1991).
[16] H. B. Stuhrmann, Adv. Polym. Sci. **67**, 123 (1985).
[17] J. Bordas, M. H. J. Koch, P. H. Clout, E. Dorrington, C. Boulin, and A. Gabriel, J. Phys. E **13**, 938 (1980).
[18] M. H. J. Koch and J. Bordas, Nucl. Instrum. Methods **208**, 461 (1983).
[19] S. Bras, A. Craievich, J. M. Sanchez, C. Williams, and E. D. Zanotto, Nucl. Instrum. Methods **208**, 489 (1983).

[20] M. Caffrey and D. H. Bilderback, Nucl. Instrum. Methods **208**, 495 (1983).
[21] W. Bras, G. E. Derbyshire, A. J. Ryan, G. R. Mant, A. Felton, R. A. Lewis, C. J. Hall, and G. N. Greaves, Nucl. Instrum. Methods A **326**, 587 (1993).
[22] B. Chu, D.-Q. Wu, and C. Wu, Rev. Sci. Instrum. **58**, 1158 (1987).
[23] S. M. Gruner, Rev. Sci. Instrum. **60**, 1545 (1989).
[24] J. Widom and H.-P. Feng, Rev. Sci. Instrum. **60**, 3231 (1989).
[25] H. F. Fuchs, D. Q. Wu, and B. Chu, Rev. Sci. Instrum. **61**, 712 (1990).
[26] E. F. Eikenberry, S. M. Gruner, and J. L. Lowrance, IEEE Trans. Nucl. Sci. **83**, 542 (1986).
[27] C. Brizard and B. Rodricks, Rev. Sci. Instrum. **63**, 802 (1992).
[28] P. M. Epperson and M. B. Deuton, Anal. Chem. **61**, 1513 (1989).
[29] M. G. Strauss, I. Naday, I. S. Sherman, M. R. Kraimer, E. M. Westbrook, and N. J. Zaluzec, Nucl. Instrum. Methods A **266**, 563 (1988).
[30] L. K. Turner, D. S. Mantus, Y.-C. Ling, M. T. Bernius, and G. H. Morrison, Rev. Sci. Instrum. **60**, 886 (1989).
[31] A. Guinier and G. Fournet, *Small-Angle Scattering of X rays* (Wiley, New York, 1955).
[32] T. Gao, Y. Li, J. Rousseau, K. Linliu, and B. Chu, Rev. Sci. Instrum. **64**, 390 (1993).
[33] M. Stanton, W. C. Phillips, Y. Li, and K. Kalata, J. Appl. Cryst. **25**, 549 (1992).
[34] S. M. Gruner, J. R. Milch, and G. T. Reynolds, IEEE Trans. Nucl. Sci. **25**, 562 (1978).
[35] U. W. Arndt, J. Appl. Cryst. **19**, 145 (1986).
[36] H. W. Deckman and S. M. Gruner, Nucl. Instrum. Methods A **246**, 527 (1986).